

# Correlated vibration–solvent and Duschinsky effects on electron transfer dynamics and optical spectroscopy

Zi-Fan Zhu, Yu Su, Yao Wang,\* and Rui-Xue Xu†

Hefei National Laboratory, University of Science and Technology of China, Hefei, Anhui 230088, China and  
Hefei National Research Center for Physical Sciences at the Microscale and Department of Chemical Physics,  
University of Science and Technology of China, Hefei, Anhui 230026, China

YiJing Yan

Hefei National Research Center for Physical Sciences at the Microscale and Department of Chemical Physics,  
University of Science and Technology of China, Hefei, Anhui 230026, China  
(Dated: May 8, 2025)

Understanding the effects of vibrations in electron transfer (ET) dynamics and optical spectroscopies is essential to precisely interpret the role of decoherence, especially for systems embedded in solvents. In this work, we study the correlated Duschinsky and solvent effects on ET and spectroscopy. Exploited is a novel extended dissipaton-equation-of-motion (ext-DEOM) approach, which is an exact and non-Markovian, non-perturbative method for quadratic system-bath couplings. The unified bath description, in terms of multiple Brownian oscillators (BOs), comprises the solvent modes and also intramolecular vibrations. Both ET dynamics and spectroscopy show the complex interplay among linear displacements, frequency shifts, Duschinsky rotations and solvent-induced BO-mode correlations. The reduced ET system density operator evolution is further analyzed in the context of Bloch sphere representation that is basis-set independent due to its geometric nature.

## I. INTRODUCTION

Interpretations on electron transfer (ET) dynamics and optical spectroscopies are essential for exploring properties of electronic systems under the influences of vibrations and solvents.<sup>1–8</sup> In particular, the role of vibrations, where the motions of different vibrational modes are not indeed independent but correlated via the solvent, has become increasingly recognized to be crucial for an accurate investigation on properties of molecular systems. This is especially significant for solvated systems where the solvent introduces additional complexities.<sup>9–12</sup>

In many molecular systems, vibrational modes are strongly coupled to electronic transitions, and these couplings can be further influenced by the surrounding solvent. A prominent feature of solvated systems is the solvent influence on the decoherence dynamics and structures of spectral bands. This can be understood in terms of a dynamic solvation shell that responds/reorganizes to the molecular motion. Additionally, the Duschinsky effect, which arises from the rotation of the normal modes upon electronic transitions/exitations, is another critical factor.<sup>13</sup> This effect, which describes the mixing of vibrational modes between the ground and excited states, can further complicate the analysis.<sup>14–19</sup>

Despite its importance, an accurate, generalized and comprehensive theoretical framework that accounts for correlated vibrations and solvent effects remains elusive. Traditional method<sup>14</sup> treats these effects separately, leading to simplifications which may not fully capture the complexity of real molecular systems. To address this, we present a combined approach that integrates the solvent and Duschinsky effects within a unified framework, using the extended dissipaton-equation-of-motion (ext-DEOM) formalism with quadratic environment (bath)

couplings.<sup>20,21</sup> In our previous work,<sup>21</sup> only changes of frequencies of vibrational normal modes upon the electronic excitation are considered. This paper generalizes to include the Duschinsky rotations, together with the correlated solvent effects.

The DEOM formalism has been established as an exact and nonperturbative approach for open quantum systems.<sup>22,23</sup> It adopts dissipaton as quasi-particle to characterize the statistical property of thermal bath. DEOM recovers the hierarchical equations of motion (HEOM) method<sup>24–29</sup> for the reduced system dynamics. HEOM was constructed via the derivative on the Feymann–Vernon influence functional path integral,<sup>24,26,30</sup> for bath couplings satisfying Gaussian statistics modeled as harmonic oscillators linearly coupled to the system. The dissipaton theory is more convenient and straightforward for bath collective dynamics and polarizations as well as further extension to nonlinear bath couplings which is of non-Gaussian statistics.<sup>20,21,31,32</sup>

In this work, we apply the ext-DEOM to a system with two electronic states, focusing on the combined effects of correlated vibrations and solvent interactions, and the Duschinsky rotations. We show how these factors affect the ET decoherence dynamics and optical spectra. The environment is composed of intramolecular vibration modes and the solvent. To apply the ext-DEOM, one key step is to obtain the bath coupling descriptors with the linear displacement ansatz<sup>21</sup> that is generalized in this paper to include the Duschinsky rotation between multimodes. We elaborate how an accurate description can be achieved, thus offering an exact approach with the ext-DEOM to interpret both ET process and absorption spectra. Furthermore the ET decoherence dynamics is visualized via the Bloch sphere representation that is basis-

set independent due to its geometric nature. Our results highlight the importance of a comprehensive treatment of correlated vibrational and solvent effects for reliable predictions in complex systems.

The remainder of this paper is organized as follows. We present the total composed Hamiltonian in Sec. II A, and the derivation to obtain the bath coupling descriptors with the linear displacement ansatz in Sec. II B. In Sec. II C, we present the ext-DEOM formalism that will be adopted in the simulation. Numerical demonstrations are presented in Sec. III. Finally, we summarize the paper in Sec. IV. Throughout this paper, we set the Planck constant and Boltzmann constant as units ( $\hbar = 1$  and  $k_B = 1$ ), and  $\beta = 1/T$ , with  $T$  being the temperature.

## II. THEORY

In this section, we start from the Hamiltonian of total composition where the intramolecular vibrational modes involve the Duschinsky rotation upon the electronic state transition. After that we derive the linear and quadratic bath coupling descriptors via the linear displacement ansatz. The extended dissipaton formalism applied to this system is then presented.

### A. Total Hamiltonian

Consider a molecular system, consisting of two electronic states and vibrational modes  $\{\hat{q}_n\}$  and  $\{\hat{q}'_n\}$  on the ground ( $|g\rangle$ ) and the excited ( $|e\rangle$ ) surfaces, respectively, embedded in solvent environments. The total molecular composite Hamiltonian reads

$$H_{\text{tot}} = H_g|g\rangle\langle g| + (H_e + \omega_{eg})|e\rangle\langle e| + \hat{V}, \quad (1)$$

where  $\hat{V} \equiv V(|e\rangle\langle g| + |g\rangle\langle e|)$  is the interstate coupling that is assumed independent of nuclear modes. The nuclear Hamiltonians are modelled by Brownian oscillators (BOs),

$$H_g = \sum_{n=1}^N \frac{\Omega_n}{2} (\hat{p}_n^2 + \hat{q}_n^2) + \sum_{k=1}^{N_{\text{sol}}} \frac{\omega_k}{2} \left[ \tilde{p}_k^2 + \left( \tilde{x}_k - \sum_n \frac{c_{nk}}{\omega_k} \hat{q}_n \right)^2 \right], \quad (2a)$$

$$H_e = \sum_{n=1}^N \frac{\Omega'_n}{2} (\hat{p}'_n^2 + \hat{q}'_n^2) + \sum_{k=1}^{N_{\text{sol}}} \frac{\omega_k}{2} \left\{ \tilde{p}_k^2 + \left[ (\tilde{x}_k - \tilde{d}_k) - \sum_n \frac{c'_{nk}}{\omega_k} \hat{q}'_n \right]^2 \right\}, \quad (2b)$$

with  $\{\tilde{d}_k\}$  being the linear displacements of the solvent modes  $\{\tilde{x}_k\}$ . As a continuous solvent model, the solvent modes are assumed irrotational and frequencies  $\{\omega_k\}$  unchanged.

The molecular vibrational modes in two surfaces involve the displacements ( $\{d_m\}$ ), frequency shifts ( $\{\Omega'_n\}$  versus  $\{\Omega_m\}$ ), and Duschinsky rotation ( $\{\bar{S}_{nm}\}$ ), related by

$$\hat{q}'_n = \sum_m \bar{S}_{nm} (\Omega'_n / \Omega_m)^{\frac{1}{2}} (\hat{q}_m - d_m). \quad (3)$$

In matrix form it reads

$$\hat{\mathbf{q}}' = \boldsymbol{\Omega}'^{\frac{1}{2}} \bar{\mathbf{S}} \boldsymbol{\Omega}^{-\frac{1}{2}} (\hat{\mathbf{q}} - \mathbf{d}) \equiv \mathbf{S}(\hat{\mathbf{q}} - \mathbf{d}), \quad (4)$$

with  $\bar{\mathbf{S}}^T \bar{\mathbf{S}} = \mathbf{I}$ . Here

$$\mathbf{S} \equiv \boldsymbol{\Omega}'^{\frac{1}{2}} \bar{\mathbf{S}} \boldsymbol{\Omega}^{-\frac{1}{2}}, \quad (5)$$

$\boldsymbol{\Omega} = \text{diag}\{\Omega_1, \dots, \Omega_N\}$  and  $\boldsymbol{\Omega}' = \text{diag}\{\Omega'_1, \dots, \Omega'_N\}$ . For later use, we denote also  $\mathbf{S}' \equiv \boldsymbol{\Omega}^{\frac{1}{2}} \bar{\mathbf{S}}^T \boldsymbol{\Omega}'^{-\frac{1}{2}} = \mathbf{S}^{-1}$ .

In Eq. (2), we further assume the relation between the coupling coefficients

$$c'_{nk} = \sum_m S'_{nm}^T c_{mk}, \quad (6)$$

which results in

$$\sum_{nk} c'_{nk} \hat{q}'_n (\tilde{x}_k - \tilde{d}_k) = \sum_{nk} c_{nk} (\hat{q}_n - d_n) (\tilde{x}_k - \tilde{d}_k). \quad (7)$$

Physically this amounts to that the change of overall vibration–solvent interaction depends just on the displacements upon the electronic transition. The physical consideration here is based on that the solvent is a continuous fluid with infinite number of degrees of freedom. Finally we note in case that the Duschinsky effect of certain neighboring shell of solvent is not negligible, it may be treated in the way as the intramolecular modes.

To complete the BO description, we shall also characterize the response functions,

$$\chi_g(t) \equiv \{\chi_{g,mn}(t) \equiv i\langle [\hat{q}_m(t), \hat{q}_n(0)] \rangle_g\}, \quad (8)$$

Here,  $\langle \hat{O} \rangle_g \equiv \text{tr}_g(\hat{O} e^{-\beta H_g}) / \text{tr}_g(e^{-\beta H_g})$  and  $\hat{q}_m(t) \equiv e^{iH_g t} \hat{q}_m e^{-iH_g t}$ . In terms of frequency resolution,  $\tilde{f}(\omega) \equiv \int_0^\infty dt e^{i\omega t} f(t)$ , Eq. (8) is resolved as the BO form,<sup>5,33,34</sup>

$$\tilde{\chi}_g(\omega) = \left[ \boldsymbol{\Omega}^2 - \omega^2 - i\omega \tilde{\zeta}(\omega) \right]^{-1} \boldsymbol{\Omega}, \quad (9)$$

where  $\tilde{\zeta}(\omega)$  is the solvent frictional resolution.<sup>5,33</sup> For later use, we define

$$\tilde{\chi}_{g,mn}^{(+)}(\omega) \equiv [\tilde{\chi}_{g,mn}(\omega) + \tilde{\chi}_{g,nm}^*(\omega)]/2 \quad (10a)$$

and

$$\tilde{\chi}_{g,mn}^{(-)}(\omega) \equiv [\tilde{\chi}_{g,mn}(\omega) - \tilde{\chi}_{g,nm}^*(\omega)]/(2i). \quad (10b)$$

They are related via the Kramers-Kronig relation<sup>5,33</sup>

$$\tilde{\chi}_{g,mn}^{(+)}(\omega) = -\frac{1}{\pi} \mathcal{P} \int_{-\infty}^{\infty} d\omega' \frac{\tilde{\chi}_{g,mn}^{(-)}(\omega')}{\omega - \omega'} \quad (11a)$$

and

$$\tilde{\chi}_{g,mn}^{(-)}(\omega) = \frac{1}{\pi} \mathcal{P} \int_{-\infty}^{\infty} d\omega' \frac{\tilde{\chi}_{g,mn}^{(+)}(\omega')}{\omega - \omega'} \quad (11b)$$

where  $\mathcal{P}$  denotes the principle integration.

## B. Bath coupling descriptors

To apply methods concerning open systems, we need to recast the total Hamiltonian into the system-plus-environment (bath) form,  $H_{\text{tot}} = H_{\text{S}} + H_{\text{SB}} + h_{\text{B}}$ . Assuming the electronic system initially at the ground state  $|g\rangle$  equilibrated with its surroundings  $H_g$ , we rewrite Eq. (1) as

$$H_{\text{tot}} = \omega_{eg}|e\rangle\langle e| + \hat{V} + (H_e - H_g)|e\rangle\langle e| + H_g. \quad (12)$$

To continue, let us denote

$$X_n = \sum_k c_{nk} \tilde{x}_k \quad \text{and} \quad D_n = \sum_k c_{nk} \tilde{d}_k. \quad (13)$$

Inferred from Eqs. (2a) and (2b), the renormalized frequencies of BOs according to the two states are respectively

$$\tilde{\eta}_{mn} \equiv \sum_k \frac{c_{mk} c_{nk}}{\omega_k} \quad \text{and} \quad \tilde{\eta}'_{mn} \equiv \sum_k \frac{c'_{mk} c'_{nk}}{\omega_k}. \quad (14)$$

In terms of the matrix form  $\tilde{\eta}$  and  $\tilde{\eta}'$ , they are related by  $\tilde{\eta}' = \mathbf{S}'^T \tilde{\eta} \mathbf{S}'$ . We thus obtain

$$\begin{aligned} H_e - H_g &= \frac{1}{2} \hat{\mathbf{q}}^T (\mathbf{S}^T \boldsymbol{\Omega}' \mathbf{S} - \boldsymbol{\Omega}) \hat{\mathbf{q}} - \hat{\mathbf{q}}^T \mathbf{S}^T \boldsymbol{\Omega}' \mathbf{S} \mathbf{d} \\ &\quad - \hat{\mathbf{q}}^T \tilde{\eta} \mathbf{d} + \hat{\mathbf{q}}^T \mathbf{D} + \frac{1}{2} \mathbf{d}^T \mathbf{S}^T \boldsymbol{\Omega}' \mathbf{S} \mathbf{d} + \frac{1}{2} \mathbf{d}^T \tilde{\eta} \mathbf{d} \\ &\quad + \mathbf{d}^T \mathbf{X} - \tilde{\mathbf{x}}^T \boldsymbol{\omega} \tilde{\mathbf{d}} - \mathbf{d}^T \mathbf{D} + \frac{1}{2} \tilde{\mathbf{d}}^T \boldsymbol{\omega} \tilde{\mathbf{d}}. \end{aligned} \quad (15)$$

To derive the linear and quadratic bath coupling descriptors, we adopt in the following the linear displacement ansatz proposed in Ref. 21 for the case of single solvation bath mode. This ansatz arises from considering the limit that the quadratic coupling term vanishes. In the present work that is  $\bar{\mathbf{S}} = 1$  and  $\boldsymbol{\Omega}' = \boldsymbol{\Omega}$ , leading to  $\hat{\mathbf{q}}' = \hat{\mathbf{q}} - \mathbf{d}$ . The mutually coupled harmonic oscillators in Eq. (2) can be transformed into independent normal modes,  $\{\mathbf{x}_j\}$ , and displaced as  $\{\mathbf{x}_j - \bar{\mathbf{d}}_j\}$  at the  $|e\rangle$  state. We have

$$(H_e - H_g)_{\text{no quadratic}} = \sum_{j=1}^{N+N_{\text{sol}}} \left( \frac{1}{2} \bar{\omega}_j \bar{\mathbf{d}}_j^2 - \bar{\omega}_j \bar{\mathbf{d}}_j \mathbf{x}_j \right). \quad (16)$$

We can always define (mathematically a problem of more unknowns than equations/restrictions)

$$\sum_j \bar{\omega}_j \bar{\mathbf{d}}_j \mathbf{x}_j \equiv \sum_{n=1}^N (2\lambda_n \Omega_n)^{\frac{1}{2}} \sum_j \bar{c}_{nj} \mathbf{x}_j = \sum_{n=1}^N (2\lambda_n \Omega_n)^{\frac{1}{2}} \hat{q}_n, \quad (17)$$

where

$$\bar{\mathbf{d}}_j = \frac{1}{\bar{\omega}_j} \sum_{n=1}^N (2\lambda_n \Omega_n)^{\frac{1}{2}} \bar{c}_{nj}, \quad (18)$$

with  $\lambda_n$  to be determined later [cf. Eq. (24)]. At the microscopic level, the spectral density, the counterpart of Eq. (10b), reads

$$\tilde{\chi}_{g,mn}^{(-)}(\omega) = \frac{\pi}{2} \sum_j \bar{c}_{mj} \bar{c}_{nj} [\delta(\omega - \bar{\omega}_j) - \delta(\omega + \bar{\omega}_j)]. \quad (19)$$

Note that  $\tilde{\chi}_{g,mn}^{(-)}(\omega = 0) = 0$ . Therefore, due to Eq. (11a), we obtain

$$\tilde{\chi}_{g,mn}(0) = \tilde{\chi}_{g,mn}^{(+)}(0) = \frac{1}{\pi} \mathcal{P} \int_{-\infty}^{\infty} d\omega \frac{\tilde{\chi}_{g,mn}^{(-)}(\omega)}{\omega}. \quad (20)$$

Equations (19) and (20) together give

$$\tilde{\chi}_{g,mn}(0) = \sum_j \frac{\bar{c}_{mj} \bar{c}_{nj}}{\bar{\omega}_j}. \quad (21)$$

On the other hand, from Eq. (9) we have  $\tilde{\chi}_g(0) = \boldsymbol{\Omega}^{-1}$ . As a result,

$$\begin{aligned} \frac{1}{2} \sum_j \bar{\omega}_j \bar{\mathbf{d}}_j^2 &= \frac{1}{2} \sum_j \frac{1}{\bar{\omega}_j} \sum_{mn} (2\lambda_n \Omega_n)^{\frac{1}{2}} (2\lambda_m \Omega_m)^{\frac{1}{2}} \bar{c}_{mj} \bar{c}_{nj} \\ &= \sum_n \lambda_n. \end{aligned} \quad (22)$$

By Eqs. (17) and (22), Eq. (16) is thus expressed as

$$(H_e - H_g)_{\text{no quadratic}} = \sum_{n=1}^N [\lambda_n - (2\lambda_n \Omega_n)^{\frac{1}{2}} \hat{q}_n]. \quad (23)$$

By the same way of linear combination as  $\hat{q}_n = \sum_j \bar{c}_{nj} \mathbf{x}_j$ , we have [cf. Eq. (18)]

$$d_n = \sum_j \bar{c}_{nj} \bar{\mathbf{d}}_j = \sum_j \frac{\bar{c}_{nj}}{\bar{\omega}_j} \sum_m (2\lambda_m \Omega_m)^{\frac{1}{2}} \bar{c}_{mj} = \left( \frac{2\lambda_n}{\Omega_n} \right)^{\frac{1}{2}}. \quad (24)$$

With this ansatz elaborated in the above, comparing Eq. (23) to Eq. (15) at the scenario without quadratic couplings ( $\bar{\mathbf{S}} = 1$  and  $\boldsymbol{\Omega}' = \boldsymbol{\Omega}$ ), we obtain

$$\begin{aligned} \mathbf{d}^T \tilde{\eta} \mathbf{d} - 2\mathbf{d}^T \mathbf{D} + \tilde{\mathbf{d}}^T \boldsymbol{\omega} \tilde{\mathbf{d}} &= 0, \\ \mathbf{q}^T \tilde{\eta} \mathbf{d} - \mathbf{q}^T \mathbf{D} - \mathbf{d}^T \mathbf{X} + \mathbf{x}^T \boldsymbol{\omega} \tilde{\mathbf{d}} &= 0. \end{aligned} \quad (25)$$

This finishes the multi-mode generalization involving Duschinsky rotation of the linear displacement ansatz brought forward for the single-mode scenario in Ref. 21. The derivation in Ref. 21 adopts further a linear displacement mapping to obtain the descriptors. The mapping is not needed for the modeled system in this work. Note that simulations based on the full form of Eq. (15) without adopting the linear displacement ansatz can also be carried out. The treatments on the entangled vibration-solvent terms will be similar as those in Ref. 35.

By using Eq. (25), Eq. (15) then readily leads to

$$H_e - H_g = \alpha_0 + \alpha_1 \cdot \hat{\mathbf{q}} + \hat{\mathbf{q}}^T \boldsymbol{\alpha}_2 \hat{\mathbf{q}}, \quad (26)$$

with the bath coupling descriptors

$$\alpha_0 = \frac{1}{2} \mathbf{d}^T \mathbf{S}^T \boldsymbol{\Omega}' \mathbf{S} \mathbf{d}, \quad (27a)$$

$$\boldsymbol{\alpha}_1 = -\mathbf{S}^T \boldsymbol{\Omega}' \mathbf{S} \mathbf{d}, \quad (27b)$$

$$\boldsymbol{\alpha}_2 = \frac{1}{2} (\mathbf{S}^T \boldsymbol{\Omega}' \mathbf{S} - \boldsymbol{\Omega}). \quad (27c)$$

Here we assume the electronic system is initially at the ground state  $|g\rangle$  equilibrated with its surroundings  $H_g$ . For the other condition that the system is initially equilibrated at  $|e\rangle$  with  $H_e$ , there is correspondingly

$$H_{\text{tot}} = \omega_{eg} |e\rangle\langle e| + \hat{V} + (H_g - H_e) |g\rangle\langle g| + H_e, \quad (28)$$

where

$$H_g - H_e = \alpha'_0 + \boldsymbol{\alpha}'_1 \cdot \hat{\mathbf{q}}' + \hat{\mathbf{q}}'^T \boldsymbol{\alpha}'_2 \hat{\mathbf{q}}', \quad (29)$$

with bath coupling descriptors reading

$$\alpha'_0 = \frac{1}{2} \mathbf{d}^T \boldsymbol{\Omega} \mathbf{d}, \quad (30a)$$

$$\boldsymbol{\alpha}'_1 = \mathbf{S}'^T \boldsymbol{\Omega} \mathbf{d}, \quad (30b)$$

$$\boldsymbol{\alpha}'_2 = \frac{1}{2} (\mathbf{S}'^T \boldsymbol{\Omega} \mathbf{S}' - \boldsymbol{\Omega}'). \quad (30c)$$

For single-mode scenarios, Eqs. (27) and (30) reduce to the results in Ref. 21.

### C. Dissipaton theory with linear and quadratic environment couplings

The quantum dissipative dynamics method starts from the total system-plus-bath composite Hamiltonian being of the form  $H_{\text{tot}} = H_s + H_{\text{SB}} + h_{\text{B}}$ . Concerning Eqs. (12) and (26),  $H_s = (\omega_{eg} + \alpha_0) |e\rangle\langle e| + \hat{V}$  and

$$H_{\text{SB}} = \hat{Q} (\boldsymbol{\alpha}_1 \cdot \hat{\mathbf{q}} + \hat{\mathbf{q}}^T \boldsymbol{\alpha}_2 \hat{\mathbf{q}}), \quad (31)$$

where  $\hat{Q} = |e\rangle\langle e|$ . The harmonic bath  $h_{\text{B}} = H_g$  constitutes the Gauss-Wick's environment ansatz where the environmental influence is fully characterized by the correlation functions,  $\{\langle \hat{q}_m(t) \hat{q}_n(0) \rangle_{\text{B}} = \langle \hat{q}_m(t) \hat{q}_n(0) \rangle_g\}$ . They are related to the spectral densities  $\{\chi_{g;mn}^{(-)}(\omega)\}$  via the fluctuation-dissipation theorem,<sup>5</sup>

$$\begin{aligned} \langle \hat{q}_m(t) \hat{q}_n(0) \rangle_{\text{B}} &= \frac{1}{\pi} \int_{-\infty}^{\infty} d\omega \frac{e^{-i\omega t} \chi_{g;mn}^{(-)}(\omega)}{1 - e^{-\beta\omega}} \\ &\simeq \sum_{k=1}^K \eta_{mnk} e^{-\gamma_k t}, \end{aligned} \quad (32)$$

where

$$\chi_{g;mn}^{(-)}(\omega) \equiv \frac{1}{2} \int_{-\infty}^{\infty} dt e^{i\omega t} \langle [\hat{q}_m(t), \hat{q}_n(0)] \rangle_g. \quad (33)$$

The exponential series expansion of Eq. (32) can be achieved by using the time-domain Prony fitting decomposition scheme.<sup>36</sup> The time-reversal relation of correlation functions is given by

$$\langle \hat{q}_n^{\text{B}}(0) \hat{q}_m^{\text{B}}(t) \rangle_{\text{B}} = \langle \hat{q}_m(t) \hat{q}_n(0) \rangle_{\text{B}}^* = \sum_{k=1}^K \eta_{mnk}^* e^{-\gamma_k t}. \quad (34)$$

The exponents  $\{\gamma_k\}$  in Eqs. (32) and (34) must be either real or complex conjugate paired, and thus one may determine  $\bar{k}$  in the index set  $\{k = 1, 2, \dots, K\}$  by the pairwise equality  $\gamma_{\bar{k}} = \gamma_k^*$ . It is the exponential series expansion in Eqs. (32) and (34) that inspired the idea of relating each exponential mode of correlation function to a statistical quasi-particle, i.e., a *dissipaton*.<sup>22,23</sup>

The dissipaton theory begins with the *dissipatons decomposition* that reproduces the correlation function in Eqs. (32) and (34). It decomposes  $\hat{q}_m$  into a number of dissipatons,  $\{\hat{f}_{mk}\}$ , as

$$\hat{q}_m = \sum_{k=1}^K \hat{f}_{mk}, \quad (35)$$

reproducing Eq. (32) and (34) by setting

$$\langle \hat{f}_{mk}^{\text{B}}(t) \hat{f}_{nj}^{\text{B}}(0) \rangle_{\text{B}} = \delta_{kj} \eta_{mnk} e^{-\gamma_k t}, \quad (36a)$$

$$\langle \hat{f}_{nj}^{\text{B}}(0) \hat{f}_{mk}^{\text{B}}(t) \rangle_{\text{B}} = \delta_{kj} \eta_{mnk}^* e^{-\gamma_k t}, \quad (36b)$$

with  $\hat{f}_{nk}^{\text{B}}(t) \equiv e^{i h_{\text{B}} t} \hat{f}_{nk} e^{-i h_{\text{B}} t}$ . Each forward-backward pair of dissipaton correlation functions is specified by a single-exponent  $\gamma_k$ . In accordance with the dissipatons decomposition, the dynamical variables in DEOM are the dissipaton density operators (DDOs),

$$\rho_{\mathbf{n}}^{(n)}(t) \equiv \text{tr}_{\text{B}} \left[ \left( \prod_{mk} \hat{f}_{mk}^{n_{mk}} \right)^{\circ} \rho_{\text{tot}}(t) \right]. \quad (37)$$

Here,  $n = \sum_{mk} n_{mk}$ , with  $n_{mk} \geq 0$  for the bosonic dissipatons. The product of dissipaton operators inside  $(\cdots)^{\circ}$  is *irreducible*, which satisfies  $(\hat{f}_{mk} \hat{f}_{nj})^{\circ} = (\hat{f}_{nj} \hat{f}_{mk})^{\circ}$  for bosonic dissipatons. Each  $n$ -particles DDO,  $\rho_{\mathbf{n}}^{(n)}(t)$ , is associated with an ordered set of indexes,  $\mathbf{n} \equiv \{n_{mk}\}$ . Denote for later use  $\mathbf{n}_{mk}^{\pm}$  and  $\mathbf{n}_{mk,m'k'}^{\pm,\pm}$  which differ from  $\mathbf{n}$  only at the specified dissipatons with their occupation numbers  $\pm 1$ . The reduced system density operator is the zeroth-tier DDO,  $\rho_{\mathbf{0}}^{(0)}(t) = \rho_{0\dots 0}^{(0)}(t) = \rho_s(t)$ .

The equation of motion for DDOs including both linear and quadratic bath couplings, i.e., the ext-DEOM, is obtained as<sup>20,21</sup>

$$\begin{aligned} \dot{\rho}_{\mathbf{n}}^{(n)} &= - \left[ i \mathcal{L}_s + \gamma_{\mathbf{n}} + i \left( \alpha_0 + \sum_{mm'} \alpha_{2mm'} \langle \hat{q}_m \hat{q}_{m'} \rangle_{\text{B}} \right) \mathcal{A} \right] \rho_{\mathbf{n}}^{(n)} \\ &\quad - i \sum_{mk} \alpha_{1m} \left[ \mathcal{A} \rho_{\mathbf{n}_{mk}^+}^{(n+1)} + \sum_{m'} n_{m'k} \mathcal{C}_{mm'k} \rho_{\mathbf{n}_{m'k}^-}^{(n-1)} \right] \\ &\quad - i \sum_{mm'kk'} \left[ n_{mk} \mathcal{B}_{mk,m'} \rho_{\mathbf{n}_{mk,m'k'}^{+,+}}^{(n)} + \alpha_{2mm'} \mathcal{A} \rho_{\mathbf{n}_{mk,m'k'}^{+,+}}^{(n+2)} \right. \\ &\quad \left. + \alpha_{2mm'} n_{mk} (n_{m'k'} - \delta_{mm'} \delta_{kk'}) \mathcal{D}_{mm'kk'} \rho_{\mathbf{n}_{mk,m'k'}^{(-,-)}}^{(n-2)} \right]. \end{aligned} \quad (38)$$

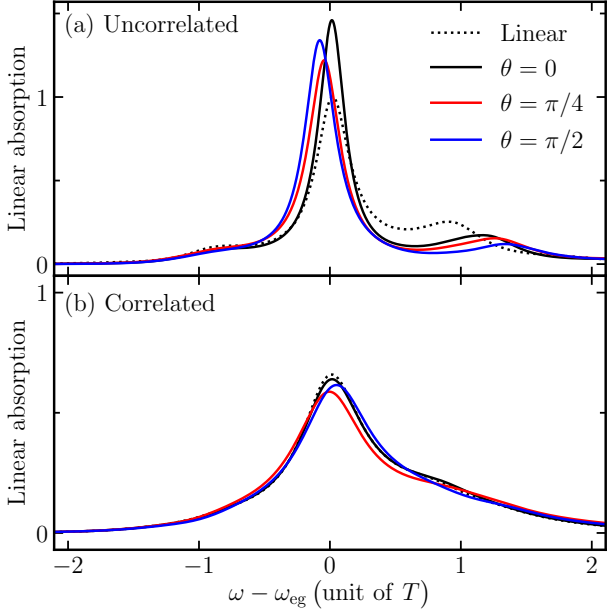


FIG. 1: The evaluated absorption spectra with two low-frequency modes. All values are uniformly scaled by the peak amplitude of linear case in (a)-panel.

Here,  $\gamma_{\mathbf{n}} \equiv \sum_{mk} n_{mk} \gamma_k$ ,  $\mathcal{L}_s \hat{O} \equiv [H_s, \hat{O}]$ ,  $\mathcal{A} \hat{O} \equiv [\hat{Q}, \hat{O}]$ , and other involved superoperators are defined as

$$\begin{aligned} \mathcal{B}_{mk, m'} \hat{O} &\equiv 2 \sum_{m''} \alpha_{2m'' m'} \mathcal{C}_{m'' mk} \hat{O}, \\ \mathcal{C}_{mm' k} \hat{O} &\equiv \eta_{mm' k} \hat{Q} \hat{O} - \eta_{mm' k}^* \hat{O} \hat{Q}, \\ \mathcal{D}_{mm' kk'} \hat{O} &\equiv \sum_{ll'} (\eta_{mlk} \eta_{m'l'k'} \hat{Q} \hat{O} - \eta_{mlk}^* \eta_{m'l'k'}^* \hat{O} \hat{Q}). \end{aligned}$$

In Eq. (38), the DDOs form a hierarchical structure with couplings not only between adjacent layers ( $n \pm 1$ ) but also between next-nearest-neighbor layers ( $n \pm 2$ ). The latter arises from the quadratic coupling term in the system-environment interaction [cf.  $\alpha_2$ -term in Eq. (31)]. Equation (38) is obtained via the dissipaton algebra, and its exactness has also been verified through comparisons with the stochastic-field method<sup>37</sup> and the core-system approach.<sup>38</sup> Notably, the ext-DEOM can be applied not only to compute real-time dynamics but also to study imaginary-time evolution and non-equilibrium thermodynamic properties.<sup>38</sup>

### III. NUMERICAL DEMONSTRATION

In the following demonstrations, we set the temperature  $T$  as the unit. We consider two vibration modes under Duschinsky transformation characterized by

$$\bar{\mathbf{S}} = \begin{pmatrix} \cos \theta & -\sin \theta \\ \sin \theta & \cos \theta \end{pmatrix}. \quad (39)$$

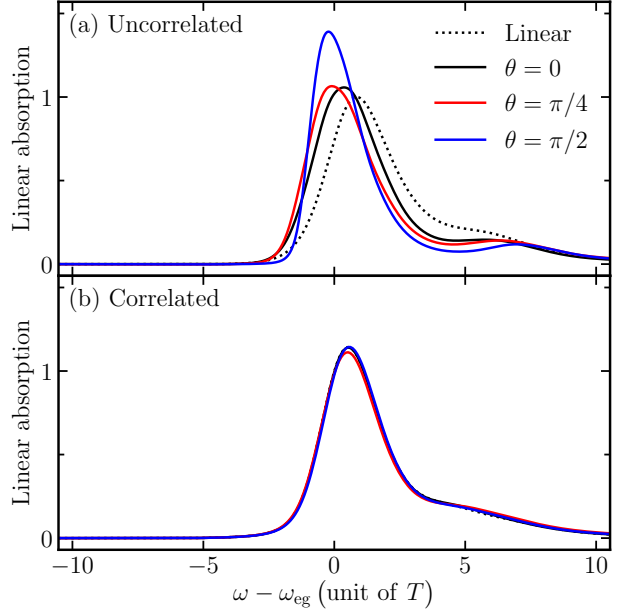


FIG. 2: The evaluated absorption spectra with two high-frequency modes and one additional overdamped BO mode. All values are uniformly scaled by the peak amplitude of linear case in (a)-panel.

We select the angle to be  $\theta = 0, \pi/4, \pi/2$ . The dimensionless displacements  $d_1$  and  $d_2$  in Eq. (3) are both selected to be  $-0.5$ . For the solvent friction influence, we assume the white-noise limit for  $\tilde{\zeta}(\omega)$  in Eq. (9), i.e.,  $\tilde{\zeta}(\omega) \approx \tilde{\zeta}(\omega = 0) = \int_0^\infty dt \zeta(t) \equiv \Gamma$ . Note that in Eq. (14),  $\tilde{\eta} = \Omega^{-1} \zeta(t = 0)$ . We will choose  $\Gamma_{11} = \Gamma_{22} = 0.3 \Omega_1$  ( $\Omega_1$  will be specified later), corresponding to underdamped cases, while  $\Gamma_{12} = \Gamma_{21} = \Gamma_{11}/2$  and  $0$  represent correlated and uncorrelated vibration-solvent cases, respectively.

#### A. Linear absorption spectroscopy

In this subsection, we focus on the absorption spectra and set  $\hat{V} = 0$  in Eq. (1). Figure 1 depicts the evaluated absorption spectra with two underdamped BO modes,  $(\Omega_1, \Omega_2)/T = (0.97, 1.16)$  and  $(\Omega'_1, \Omega'_2)/T = (1.02, 1.11)$  in the ground and excited states, respectively. Included for comparison is also the linear coupling counterpart,  $(\bar{\mathbf{S}} = 1$  and  $\Omega' = \Omega$ ). In both Fig. 1(a) and Fig. 1(b) panels, we can observe one main peak of the electronic state transition and secondary peak with additional vibrational state excitation. The positions of these peaks vary with Duschinsky rotation angle  $\theta$ . The spectra are broadened for  $\Gamma_{12} \neq 0$ ; seen from Fig. 1(b) with respect to Fig. 1(a). This indicates stronger decoherence induced by solvent induced BO modes correlation, which will be also observed in the ET dynamics (cf. Sec. III B).

Figure 2 depicts the evaluated absorption spectra with two underdamped BO modes and one additional over-

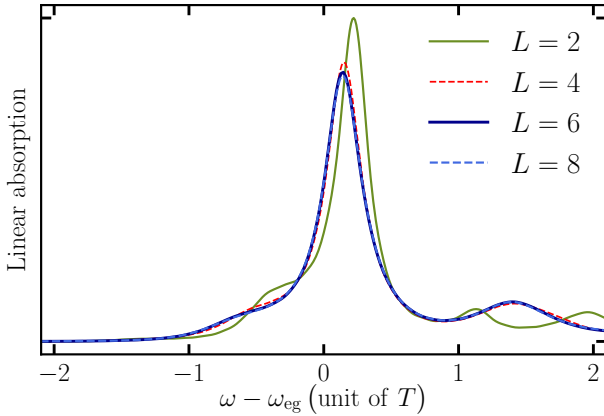


FIG. 3: The evaluated absorption spectra with different truncation tier  $L$ . The parameters are same as those in Fig. 1 with  $\theta = \pi/3$ .

damped BO mode which is neither rotated nor bath-induced correlated with the other two modes. The two underdamped BO modes are of  $(\Omega_1, \Omega_2)/T = (4.83, 5.80)$  in the ground state and  $(\Omega'_1, \Omega'_2)/T = (5.08, 5.55)$  in the excited state, with displacements  $d_1 = d_2 = -0.5$ . The overdamped mode that introduces additional broadening is of  $\Gamma_3/(2\Omega_3) = 5$ , with  $(\Omega_3, \Omega'_3)/T = (2.90, 3.15)$  and  $d_3 = -0.5$ . The peaks in Fig. 2(a) (uncorrelated scenario) still exhibit observable Duschinsky effect, with varied values of  $\theta$ , in comparison to Fig. 2(b) (correlated scenario).

In Fig. 3 we exhibit the absorption spectra, exemplified with  $\theta = \pi/3$ , calculated at different truncation tiers  $L$  by setting  $\rho^{(n>L)} = 0$  in Eq. (38). Other parameters are same as those in Fig. 1. The result of  $L = 2$  corresponds to that of the quantum master equation involving quadratic bath couplings. As an exact and nonperturbative theory, DEOM converges rather rapidly and monotonically with respect to truncation level.<sup>39</sup> Higher-frequency-shift components converge earlier. The  $L = 4$  would be enough except for the zero-frequency-shift peak, while the result of  $L = 6$  is numerically exact in the present study. All reported numerical results in this paper are converged.

Figure 4 focuses on the solvent effect in term of BO parameter,  $r_{\text{BO},i} \equiv \Gamma_{ii}/(2\Omega_i)$ , whereas gas phase scenario ( $r_{\text{BO},i} = 0$ ) has an analytical solution.<sup>14</sup> To better visualize the vibronic progression and underlying thermal effect, we consider low-frequency vibrational modes, with  $(\Omega_1, \Omega_2)/T = (0.2, 0.24)$ ,  $(\Omega'_1, \Omega'_2) = (0.21, 0.23)$  in the ground and excited states, respectively. The intrinsic richness of the spectral progression originates from the energy level disparities between the ground and excited states induced by Duschinsky rotation. Figure 4 is depicted concerning varied values of  $r_{\text{BO}}$  in the uncorrelated scenario, with  $\theta = \pi/3$ . Here, we set  $r_{\text{BO}} = r_{\text{BO},1} = r_{\text{BO},2}$  for both modes. For the gas phase,  $r_{\text{BO}} = 0$ , the spectrum is evaluated via the analytical solution in Ref. 14, phenomenologically broadened by an electronic dephasing,

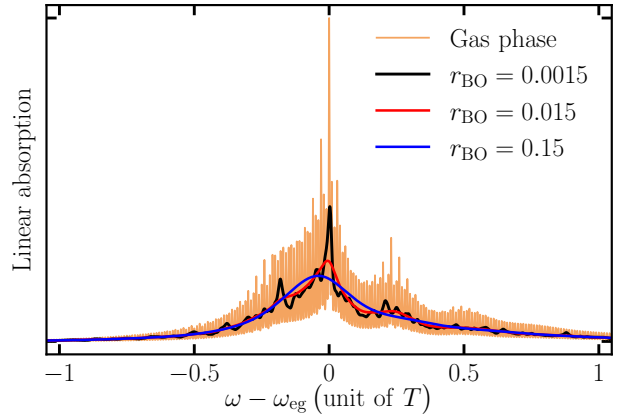


FIG. 4: The evaluated absorption spectra with different  $r_{\text{BO}}$  in uncorrelated scenario. See the text for details of parameters. All values are uniformly scaled by the peak amplitude of gas-phase case.

with  $\omega_{eg}$  being replaced by  $\omega_{eg} - i\gamma$ , where  $\gamma/T = 0.0016$ . Figure 4 illustrates the solvent effect on absorption spectra, which is not phenomenological but evaluated based on quantum dissipation theory, here via Eq. (38) with Eq. (27). The method is applicable to realistic molecules in solvents combined with quantum chemistry calculations and molecular dynamics.<sup>19,29,32,40,41</sup>

## B. Electron transfer dynamics

In this subsection, we consider the coherent ET process. We set  $\omega_{eg}/T = -2$  and  $V/T = 1$  [cf. Eq. (1)]. The other parameters are the same as those in Fig. 1. The system was initially in the ground state  $|g\rangle$ , with  $P_g(t) - P_e(t) \equiv \langle g|\rho_s(t)|g\rangle - \langle e|\rho_s(t)|e\rangle$ , the population difference between the ground and excited states, initially being 1. The evaluated  $\rho_s(t)$  can be instantaneously diagonalized into

$$\rho_s(t) = P_+(t)|\psi_+(t)\rangle\langle\psi_+(t)| + P_-(t)|\psi_-(t)\rangle\langle\psi_-(t)|, \quad (40)$$

where  $|\psi_{\pm}(t)\rangle$  denotes the instantaneous canonical basis. This directly leads to the von Neumann entropy,

$$\begin{aligned} S_{\text{vN}}(t) &\equiv -\text{tr}_s[\rho_s(t) \ln \rho_s(t)] \\ &= -P_+(t) \ln P_+(t) - P_-(t) \ln P_-(t). \end{aligned} \quad (41)$$

Figure 5 depicts the transfer evolution in terms of  $P_g(t) - P_e(t)$  [panels (a) and (b)] and  $P_+(t) - P_-(t)$  [panels (c) and (d)] in both uncorrelated and correlated scenarios, together with the von Neumann entropy evolution [panels (e) and (f)]. In both linear (thin-olive) and  $\theta = 0$  (black) cases, the correlated solvent effects on BO modes accelerate the transfer process to equilibrium, as observed comparing the right panels to the left ones. For  $\theta = \pi/4$  (red), i.e.  $\hat{q}'_1 \sim \hat{q}_1 - \hat{q}_2$  and  $\hat{q}'_2 \sim \hat{q}_1 + \hat{q}_2$  [cf. Eqs. (3) and (39)], the solvent-induced BO-mode correlation significantly suppresses the ET rate. In contrast,

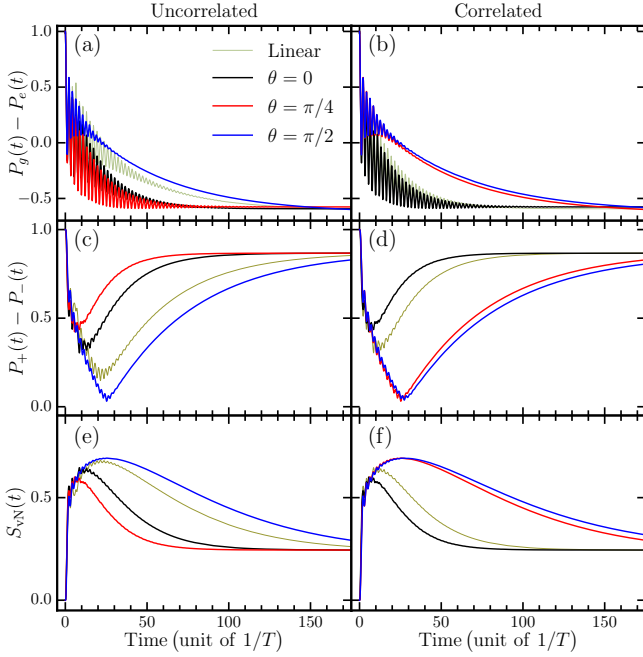


FIG. 5: Transfer evolution in terms of  $P_g - P_e$  [panels (a) and (b)] and  $P_+ - P_-$  [panels (c) and (d)], together with the evolution of von Neumann entropy [panels (e) and (f)]. See the text for details. Shown in the left and right panels are the uncorrelated and correlated scenarios, respectively.

the case of  $\theta = \pi/2$  (blue),  $\hat{q}'_1 \sim -\hat{q}_2$  and  $\hat{q}'_2 \sim \hat{q}_1$ , which is of the slowest ET behavior, exhibits minimal differences between correlated and uncorrelated scenarios. As demonstrated above, the transfer dynamics exhibit the complex interplay between Duschinsky rotation and solvent-induced BO-mode correlation.

The complete description of  $\rho_s(t)$  can go with Bloch sphere representation, in terms of

$$r_i(t) \equiv \text{tr}_s[\hat{\sigma}_i \rho_s(t)], \quad i = x, y, z \quad (42)$$

with  $\hat{\sigma}_i$  being the Pauli matrices. The Bloch sphere is a geometric representation of the state space of a two-level quantum system (qubit). Any pure state can be written as

$$|\psi\rangle_s = \cos\left(\frac{\vartheta}{2}\right)|g\rangle + e^{i\varphi}\sin\left(\frac{\vartheta}{2}\right)|e\rangle, \quad (43)$$

where  $\vartheta \in [0, \pi]$  and  $\varphi \in [0, 2\pi]$ , and corresponds to a point on the surface of the unit sphere in  $\mathbb{R}^3$  with coordinates  $(r_x, r_y, r_z) = (\sin \vartheta \cos \varphi, \sin \vartheta \sin \varphi, \cos \vartheta)$ . Two endpoints of a diameter correspond to two orthogonal wavefunctions.

More generally, any mixed state can be represented by a density matrix

$$\rho_s = \frac{1}{2}(\hat{I} + \mathbf{r} \cdot \hat{\boldsymbol{\sigma}}), \quad (44)$$

where  $\mathbf{r} = (r_x, r_y, r_z)$  is called the Bloch vector,  $\hat{\boldsymbol{\sigma}} = (\hat{\sigma}_x, \hat{\sigma}_y, \hat{\sigma}_z)$  are the Pauli matrices, and the condition

$|\mathbf{r}| \leq 1$  ensures the positivity of  $\rho_s$ . Pure states lie on the surface of the sphere (i.e.  $|\mathbf{r}| = 1$ ), while mixed states occupy the interior ( $|\mathbf{r}| < 1$ ), and the completely mixed state of maximum entropy corresponds to  $\mathbf{r} = 0$ . If a mixed state  $\rho_s$  is a convex combination,

$$\rho_s = p\rho_1 + (1-p)\rho_2, \quad (45)$$

the Bloch vector  $\mathbf{r}$  is the weighted average:

$$\mathbf{r} = p\mathbf{r}_1 + (1-p)\mathbf{r}_2, \quad (46)$$

i.e.,  $\mathbf{r}$  is located on the line segment connecting  $\mathbf{r}_1$  and  $\mathbf{r}_2$ , satisfying  $|\mathbf{r} - \mathbf{r}_2|/|\mathbf{r}_1 - \mathbf{r}_2| = p$  (law of the lever). These properties help us visualize the transfer dynamics. The Bloch sphere representation can be generalized to  $N$ -level systems, with the Bloch vector belonging to an  $(N^2 - 1)$ -dimension real space.<sup>42</sup>

Figure 6 depicts the evolution of  $\rho_s(t)$ , for uncorrected and correlated scenarios, in term of  $\mathbf{r} = (r_x, r_y, r_z)$  by the Bloch sphere representation with varied Duschinsky rotation angles, as well as the linear coupling case. Demonstrated in Fig. 7 and Fig. 8 are the corresponding evolutions of the instantaneously diagonalized basis  $|\psi_+\rangle$  and  $|\psi_-\rangle$ , respectively [cf. Eq. (40)]. These three figures can be interpreted via law of the lever, together with Fig. 5(c) and Fig. 5(d). That is at each moment the point in Fig. 6 relates to the corresponding points in Fig. 7 and Fig. 8 via law of the lever, with lever lengths being  $P_\pm(t)$  which have been indicated in Fig. 5(c) and Fig. 5(d), for uncorrected and correlated scenarios, respectively. As illustrated, the coherent ET dynamics exhibit distinct Duschinsky-angular dependence under uncorrected versus correlated scenarios. For the uncorrected scenario, the coherence time is enhanced with Duschinsky rotation angle  $\theta$  increased. In the correlated scenario, the decoherence is uniformly accelerated, and demonstrates angular insensitivity. These are consistent with the spectral behavior exhibited in Fig. 1. It is also observed that the Bloch sphere representation provides remarkable advantages for intuitively studying the coherent ET dynamics and furthermore entangled properties in qubits. Its extension to multi-level systems also facilitates the development of quantum computing models based on various numeral systems.<sup>42</sup>

#### IV. SUMMARY

We apply the extended dissipaton-equation-of-motion (ext-DEOM) method to simulate the linear absorption spectra and electron transfer (ET) dynamics involving solvent-induced BO-mode correlation and Duschinsky effects. The ext-DEOM is an exact and non-Markovian, non-perturbative approach to handle nonlinear bath couplings which are caused in this paper mainly by the Duschinsky rotation. Elaborated also is the detail on how to disassemble the total composite Hamiltonian, which can be constructed for realistic solvated molecules via

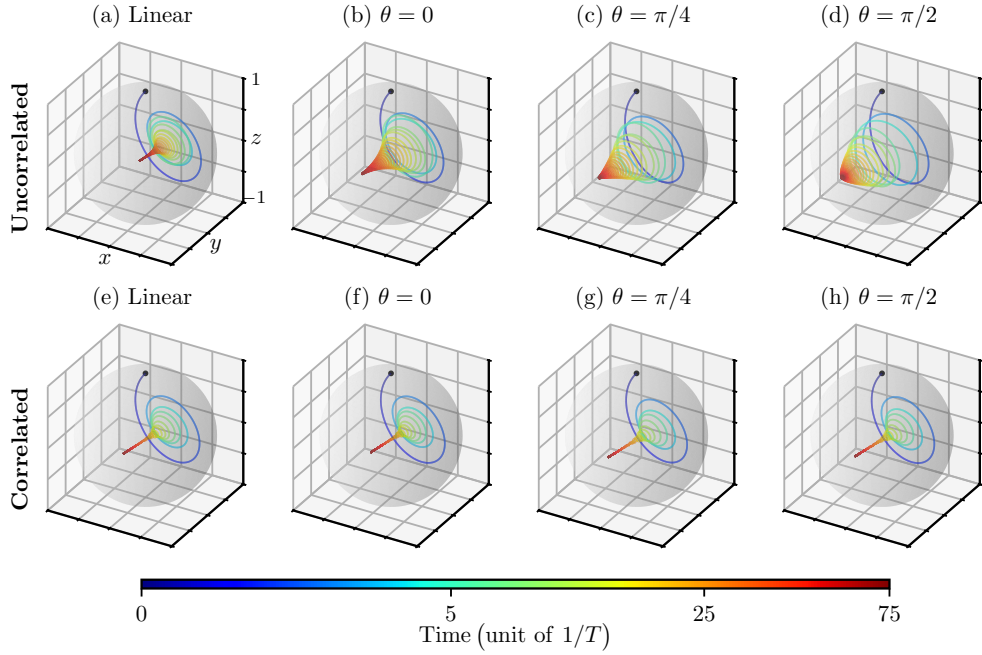


FIG. 6: The evolution of  $\rho_s(t)$  represented via Bloch sphere with varied Duschinsky rotation angles, as well as the linear coupling case. Shown in the upper and lower panels are the uncorrelated and correlated scenarios, respectively.

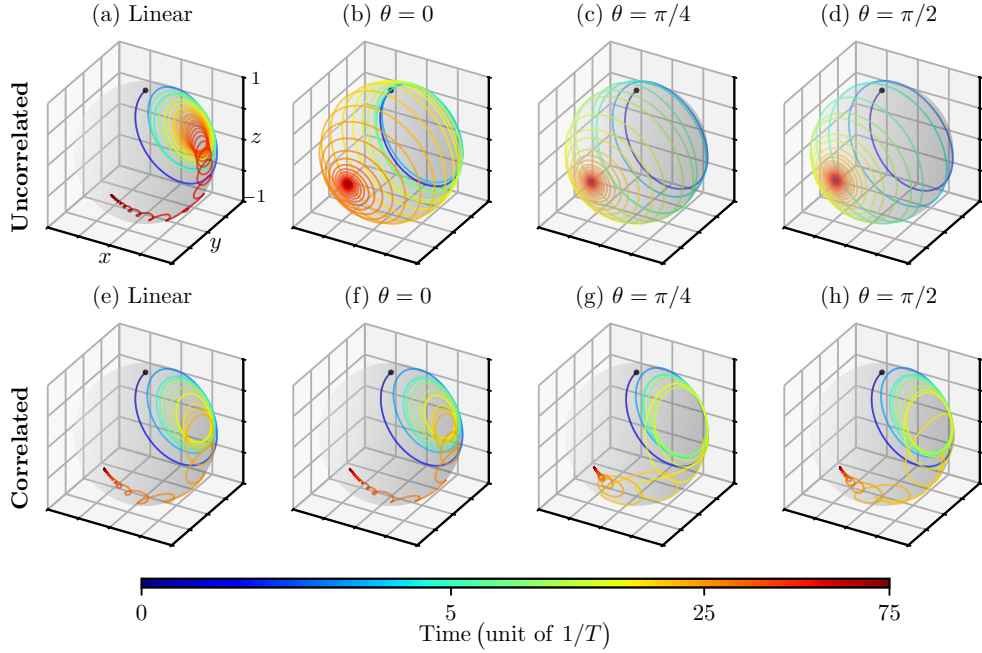


FIG. 7: The evolution of instantaneous diagonalized basis,  $|\psi_+(t)\rangle$ , with varied Duschinsky rotation angles, as well as the linear coupling case. Shown in the upper and lower panels are the uncorrelated and correlated scenarios, respectively.

quantum chemistry calculations, into system-plus-bath form with characterized bath coupling descriptors. The complexity and the importance of a comprehensive interplay between solvent-induced BO-mode correlation and Duschinsky effects are illustrated. It shows that precise evaluation is necessary for the reliable analysis and prediction of optical spectra and coherent transfer dynamics

in complex systems.

Finally, it is worth noting that the ext-DEOM method employed in this study can be not only applied to spectroscopy and transfer dynamics, but also extended to address problems in both equilibrium and non-equilibrium thermodynamics.<sup>38</sup> Not only its bosonic but also fermionic versions<sup>20,21,31</sup> have been developed and

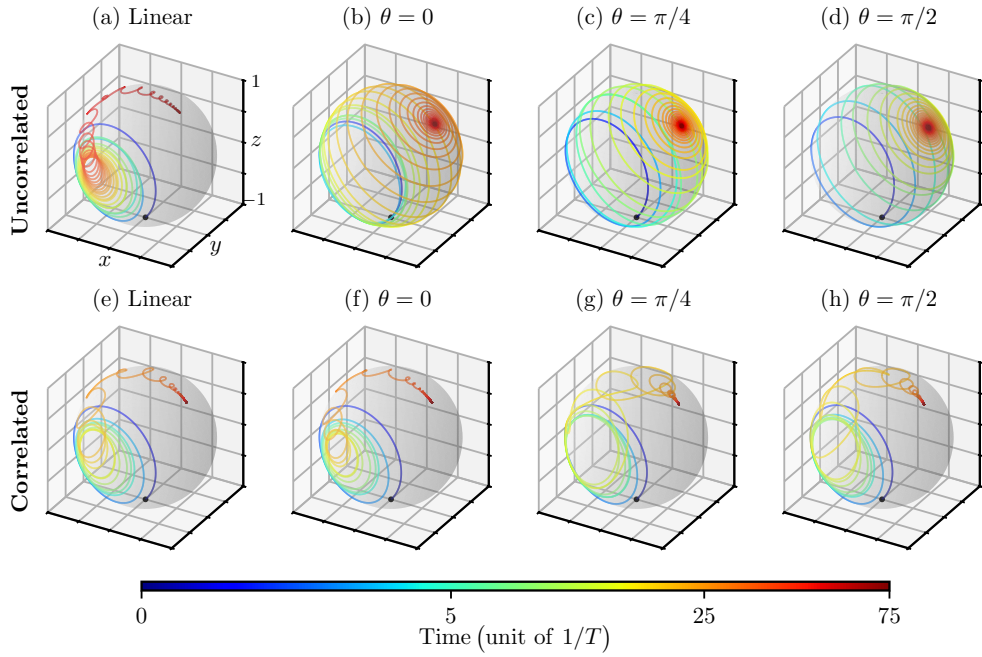


FIG. 8: The evolution of instantaneous diagonalized basis,  $|\psi_-(t)\rangle$ , with varied Duschinsky rotation angles, as well as the linear coupling case. Shown in the upper and lower panels are the uncorrelated and correlated scenarios, respectively.

the latter has been utilized to study the characteristics of an adatom in functional materials.<sup>32</sup> The method can also be applied to study and modulate the effects of high-order environmental noise in quantum computing devices.<sup>43–46</sup>

National Natural Science Foundation of China (Grant Nos. 22173088, 22373091, 224B2305), and the Innovation Program for Quantum Science and Technology (Grant No. 2021ZD0303301) is gratefully acknowledged.

### Acknowledgments

Support from the Ministry of Science and Technology of China (Grant No. 2021YFA1200103), the Na-

\* Electronic address: wy2010@ustc.edu.cn

† Electronic address: rxxu@ustc.edu.cn

<sup>1</sup> A. Nitzan, *Chemical Dynamics in Condensed Phases: Relaxation, Transfer and Reactions in Condensed Molecular Systems*, Oxford University Press, New York, 2006.

<sup>2</sup> S. Mukamel, *The Principles of Nonlinear Optical Spectroscopy*, Oxford University Press, New York, 1995.

<sup>3</sup> M. D. Levenson and S. S. Kano, *Introduction to Nonlinear Laser Spectroscopy*, Academic Press, New York, 1988.

<sup>4</sup> G. R. Fleming, *Chemical Applications of Ultrafast Spectroscopy*, Oxford University Press, New York, 1986.

<sup>5</sup> U. Weiss, *Quantum Dissipative Systems*, World Scientific, Singapore, 2021, 5th edition.

<sup>6</sup> A. Nitzan, “Phenomenology of resonance Raman scattering and resonance fluorescence from thermally relaxing systems,” *Chem. Phys.* **41**, 163 (1979).

<sup>7</sup> A. Nitzan, “Activated rate processes in condensed phases: The Kramers theory revisited,” *Adv. Chem. Phys.* **70**, 489 (1988).

<sup>8</sup> A. Nitzan, J. Jortner, J. Wilkie, A. L. Burin, and M. A. Ratner, “Tunneling Time for Electron Transfer Reactions,” *J. Phys. Chem. B* **104**, 5661 (2000).

<sup>9</sup> G. J. Small, “Persistent Nonphotochemical hole burning and the dephasing of impurity electronic transitions in organic glasses,” in *Spectroscopy and Excitation Dynamics of Condensed Molecular Systems*, edited by V. M. Agranovich and R. M. Hochstrasser, page 515, North-Holland Publishing Company, Amsterdam, 1983.

<sup>10</sup> W. H. Hesselink and D. A. Wiersma, “Theory and experimental aspects of photon echoes in molecular solids,” in *Spectroscopy and Excitation Dynamics of Condensed Molecular Systems*, edited by V. M. Agranovich and R. M. Hochstrasser, page 249, North-Holland, Amsterdam, 1983.

<sup>11</sup> E. Neria and A. Nitzan, “Simulations of solvation dynamics in simple polar solvents,” *J. Chem. Phys.* **96**, 5433 (1992).

<sup>12</sup> R. Olander and A. Nitzan, “Solvation dynamics in dielectric solvents with restricted molecular rotations:

Polyethers,” *J. Chem. Phys.* **102**, 7180 (1995).

<sup>13</sup> F. Duschinskii, “Zur Deutung der Elektronenspektren mehratomiger Moleküle,” *Acta Physicochim. URSS* **7**, 551 (1937).

<sup>14</sup> Y. J. Yan and S. Mukamel, “Eigenstate-free, Green function: Calculation of molecular absorption and fluorescence line shapes,” *J. Chem. Phys.* **85**, 5908 (1986).

<sup>15</sup> Q. Peng, Y. P. Yi, Z. G. Shuai, and J. S. Shao, “Excited state radiationless decay process with Duschinsky rotation effect: formalism and implementation,” *J. Chem. Phys.* **126**, 114302 (2007).

<sup>16</sup> F. Santoro, A. Lami, R. Imrota, J. Bloino, and V. Barone, “Effective method for the computation of optical spectra of large molecules at finite temperature including the Duschinsky and Herzberg–Teller effect: The Qx band of porphyrin as a case study,” *J. Chem. Phys.* **128**, 224311 (2008).

<sup>17</sup> H. L. Ma, J. Liu, and W. Z. Liang, “Time-Dependent Approach to Resonance Raman Spectra Including Duschinsky Rotation and Herzberg–Teller Effects: Formalism and Its Realistic Applications,” *J. Chem. Theory Comput.* **8**, 4474 (2012).

<sup>18</sup> F. J. Avila Ferrer, V. Barone, C. Cappelli, and F. Santoro, “Duschinsky, Herzberg–Teller, and multiple electronic resonance interferential effects in resonance Raman spectra and excitation profiles. The case of pyrene,” *J. Chem. Theory Comput.* **9**, 3597 (2013).

<sup>19</sup> Y. H. Wang, J. J. Ren, W. T. Li, and Z. G. Shuai, “Hybrid quantum-classical boson sampling algorithm for molecular vibrationally resolved electronic spectroscopy with Duschinsky rotation and anharmonicity,” *J. Phys. Chem. Lett.* **13**, 6391 (2022).

<sup>20</sup> R. X. Xu, Y. Liu, H. D. Zhang, and Y. J. Yan, “Theory of quantum dissipation in a class of non-Gaussian environments,” *Chin. J. Chem. Phys.* **30**, 395 (2017).

<sup>21</sup> R. X. Xu, Y. Liu, H. D. Zhang, and Y. J. Yan, “Theories of quantum dissipation and nonlinear coupling bath descriptors,” *J. Chem. Phys.* **148**, 114103 (2018).

<sup>22</sup> Y. J. Yan, “Theory of open quantum systems with bath of electrons and phonons and spins: Many-dissipaton density matrixes approach,” *J. Chem. Phys.* **140**, 054105 (2014).

<sup>23</sup> Y. Wang and Y. J. Yan, “Quantum mechanics of open systems: Dissipaton theories,” *J. Chem. Phys.* **157**, 170901 (2022).

<sup>24</sup> Y. Tanimura, “Nonperturbative expansion method for a quantum system coupled to a harmonic-oscillator bath,” *Phys. Rev. A* **41**, 6676 (1990).

<sup>25</sup> Y. A. Yan, F. Yang, Y. Liu, and J. S. Shao, “Hierarchical approach based on stochastic decoupling to dissipative systems,” *Chem. Phys. Lett.* **395**, 216 (2004).

<sup>26</sup> R. X. Xu, P. Cui, X. Q. Li, Y. Mo, and Y. J. Yan, “Exact quantum master equation via the calculus on path integrals,” *J. Chem. Phys.* **122**, 041103 (2005).

<sup>27</sup> J. S. Jin, X. Zheng, and Y. J. Yan, “Exact dynamics of dissipative electronic systems and quantum transport: Hierarchical equations of motion approach,” *J. Chem. Phys.* **128**, 234703 (2008).

<sup>28</sup> Y. Tanimura, “Numerically “exact” approach to open quantum dynamics: The hierarchical equations of motion (HEOM),” *J. Chem. Phys.* **153**, 020901 (2020).

<sup>29</sup> D. C. Zhang, L. Z. Ye, J. A. Cao, Y. Wang, R. X. Xu, X. Zheng, and Y. J. Yan, “HEOM-QUICK2: A general-purpose simulator for fermionic many-body open quantum systems—An update,” *WIREs Comput. Mol. Sci.* **14**, e1727 (2024).

<sup>30</sup> R. P. Feynman and F. L. Vernon, Jr., “The theory of a general quantum system interacting with a linear dissipative system,” *Ann. Phys.* **24**, 118 (1963).

<sup>31</sup> Y. Su, Z.-H. Chen, Y. Wang, X. Zheng, R.-X. Xu, and Y. Yan, “Extended dissipaton equation of motion for electronic open quantum systems: Application to the Kondo impurity model,” *J. Chem. Phys.* **159**, 024113 (2023).

<sup>32</sup> Y. Su, Y. Wang, Z. F. Zhu, Y. Kong, R. X. Xu, X. Zheng, and Y. J. Yan, “Extended dissipaton theory with application to adatom–graphene composite,” *J. Chem. Theo. Comput.* **21**, 4107 (2025).

<sup>33</sup> Y. J. Yan and R. X. Xu, “Quantum mechanics of dissipative systems,” *Annu. Rev. Phys. Chem.* **56**, 187 (2005).

<sup>34</sup> X.-H. Tong, H. Gong, Y. Wang, R.-X. Xu, and Y. Yan, “Multimode Brownian oscillators: Exact solutions to heat transport,” *J. Chem. Phys.* **159**, 024117 (2023).

<sup>35</sup> Z. H. Chen, Y. Wang, R. X. Xu, and Y. J. Yan, “Correlated vibration-solvent effects on the non-Condon exciton spectroscopy,” *J. Chem. Phys.* **154**, 244105 (2021).

<sup>36</sup> Z. H. Chen, Y. Wang, X. Zheng, R. X. Xu, and Y. J. Yan, “Universal time-domain Prony fitting decomposition for optimized hierarchical quantum master equations,” *J. Chem. Phys.* **156**, 221102 (2022).

<sup>37</sup> Z. H. Chen, Y. Wang, R. X. Xu, and Y. J. Yan, “Quantum dissipation with nonlinear environment couplings: Stochastic fields dressed dissipaton equation of motion approach,” *J. Chem. Phys.* **155**, 174111 (2021).

<sup>38</sup> Z.-H. Chen, Y. Wang, R.-X. Xu, and Y. Yan, “Open quantum systems with nonlinear environmental backactions: Extended dissipaton theory vs core-system hierarchy construction,” *J. Chem. Phys.* **158**, 074102 (2023).

<sup>39</sup> Z. H. Li, N. H. Tong, X. Zheng, D. Hou, J. H. Wei, J. Hu, and Y. J. Yan, “Hierarchical Liouville-space approach for accurate and universal characterization of quantum impurity systems,” *Phys. Rev. Lett.* **109**, 266403 (2012).

<sup>40</sup> L. P. Chen, R. H. Zheng, Y. Y. Jing, and Q. Shi, “Simulation of the two-dimensional electronic spectra of the Fenna–Matthews–Olson complex using the hierarchical equations of motion method,” *J. Chem. Phys.* **134**, 194508 (2011).

<sup>41</sup> Y. C. Wang, Y. L. Ke, and Y. Zhao, “The hierarchical and perturbative forms of stochastic Schrödinger equations and their applications to carrier dynamics in organic materials,” *WIREs Comput. Mol. Sci.* **9**, e1375 (2019).

<sup>42</sup> G. Kimura, “The Bloch vector for N-level systems,” *Phys. Lett. A* **314**, 339 (2003).

<sup>43</sup> C. P. Moca, I. Weymann, M. A. Werner, and G. Zaránd, “Kondo cloud in a superconductor,” *Phys. Rev. Lett.* **127**, 186804 (2021).

<sup>44</sup> Z. Han, S. A. Kivelson, and P. A. Volkov, “Quantum bipolaron superconductivity from quadratic electron-phonon coupling,” *Phys. Rev. Lett.* **132**, 226001 (2024).

<sup>45</sup> A. Blais, A. L. Grimsmo, S. M. Girvin, and A. Wallraff, “Circuit quantum electrodynamics,” *Rev. Mod. Phys.* **93**, 025005 (2021).

<sup>46</sup> P. Krantz, M. Kjaergaard, F. Yan, T. P. Orlando, S. Gustavsson, and W. D. Oliver, “A quantum engineer’s guide to superconducting qubits,” *Appl. Phys. Rev.* **6**, 021318 (2019).